Modeling the Pile Cycle of an Axially Loaded Pile in Sensitive Natural Clay

Citation for the original published paper (version of record):
Isaksson, J., Dijkstra, J. (2025). Modeling the Pile Cycle of an Axially Loaded Pile in Sensitive Natural Clay. Journal of Geotechnical and Geoenvironmental Engineering - ASCE, 151(7). http://dx.doi.org/10.1061/JGGEFK.GTENG-13179

ASCE

Modeling the Pile Cycle of an Axially Loaded Pile in Sensitive Natural Clay

Jonatan Isaksson[1] and Jelke Dijkstra[2]

Abstract: The pile cycle of an axially loaded displacement pile in a sensitive natural clay has been modeled using a coupled finite-element code for large deformations. The originality lies in the effective stress–based analysis with a consistent set of model parameters that considers all necessary soft soil features, i.e., anisotropy, destructuration, and rate dependency. Furthermore, the modeling approach is successfully benchmarked at all stages of the pile cycle (initialization, installation, equalization, loading). The benchmarking consisted of model calibration at element level, model selection using simulated and measured cone penetration test (CPTu) data, comparisons of measured and computed radial and shear stress during pile installation, and pile load testing. The results indicate that, with the exception of the absolute magnitude of the excess pore-water pressures generated during installation, the trends observed in the experimental data were captured well at all stages. Furthermore, several aspects of large deformation modeling of CPTu penetration, and pile installation were discussed. Most importantly, the difficulty in modeling the postpeak softening behavior and the balancing effects of the viscoplastic response (rate dependence) and strain-softening (destructuration) was highlighted. Finally, the empirical relation between the CPTu response and the bearing capacity of pile could be numerically confirmed. In conclusion, a first step is provided for the inclusion of the spatiotemporal response of sensitive natural clay over the full pile cycle in system-level geotechnical finite-element analysis. **DOI: 10.1061/JGGEFK.GTENG-13179.**

Introduction

The geotechnical aspects of civil engineering projects are becoming increasingly more challenging. One of the main challenges is to limit the damage to the foundations of existing, often historic, structures and to analyze their response when building in urban areas. Therefore, there is a need for system-level analyses that enable the quantification of the spatiotemporal interactions between the natural clay and the new and existing structures. Finite-element analysis has commonly been used to study these interactions at the system level over the life span, e.g., Bodas Freitas et al. (2015) of geotechnical structures (Korff et al. 2016; Stanier and White 2019; Franza et al. 2021; Tornborg et al. 2023; Singh et al. 2022). An outstanding problem in geotechnical Finite Element Analysis is the incorporation of (the effects of) large deformations associated with the installation of displacement piles (Wang et al. 2015).

Deep foundations in deposits of soft natural clay commonly use displacement piles, i.e., in Sweden, they represent up to 60% of the piles installed (Pålkommisionen 2023). During pile installation, the natural clay is displaced and distorted. The hydromechanical response of soft natural clays, in their natural undisturbed state, is characterized by features such as consolidation, rate dependency (both from generation of pore water pressures and creep), strain softening (destructuration), and (strength and stiffness) anisotropy (Casagrande and Wilson 1951; Leroueil et al. 1979; Tavenas and Leroueil 1977; Burland 1990). Hence, the state (i.e., the effective stress, the preconsolidation pressure, the excess pore water pressures, the degree of bonding, and the orientation of the fabric) evolves during and after installation. The immediate and long-term impact of the installation of displacement piles in (soft) clays has been studied extensively (e.g., Torstensson 1973; Bozozuk et al. 1978; Roy et al. 1981; Azzouz and Morrison 1988; Lehane 1992). Those findings led to the introduction of four stages and their corresponding intermediate states in the soil (Randolph and Gourvenec 2011):

1. Initial state in situ prior to pile installation;
2. Pile installation;
3. Equalization of excess pore water pressures and ongoing creep/relaxation; and
4. Loading of the pile head.

The response of soft natural clays is strongly linked to the initial state in situ before the hydromechanical loading. The K_0 condition (the ratio of horizontal and vertical effective stress), the apparent preconsolidation pressure, and the magnitude of (excess) pore water pressures all control the response upon subsequent loading of the pile. During pile installation, the clay adjacent to the pile is subjected to high loading rates that induce large shear strains. Furthermore, large excess pore water pressures are generated during this largely undrained response (Randolph et al. 1979; Roy et al. 1981). In natural sensitive clays, the large strains lead to softening of the material. The softening in natural clays is linked to the loss of bonding and the rearrangement of the initial fabric (Burland 1990). Thus, the clay in the vicinity of the pile will be in a remolded state (Karlsrud and Haugen 1985).

Subsequently, in the equalization stage, the effective stresses in the clay recover due to the dissipation of the excess pore water pressures that were generated during installation. In addition, relaxation and creep continue to change the state in the clay after the dissipation of excess pore water pressures has finished. The latter

[1]Ph.D. Student, Dept. of Architecture and Civil Engineering, Chalmers Univ. of Technology, Gothenburg SE 41296, Sweden; Engineer, Dept. of Research and Innovation, NCC Sverige AB, Herrjärva Torg 4, Solna 17080, Sweden (corresponding author). ORCID: https://orcid.org/0000-0003-1863-1508. Email: jonatan.isaksson@chalmers.se

[2]Professor, Dept. of Architecture and Civil Engineering, Chalmers Univ. of Technology, Gothenburg SE 41296, Sweden. Email: jelke.dijkstra@chalmers.se

Note. This manuscript was submitted on July 1, 2024; approved on December 27, 2024; published online on May 5, 2025. Discussion period open until October 5, 2025; separate discussions must be submitted for individual papers. This paper is part of the ***Journal of Geotechnical and Geoenvironmental Engineering***, © ASCE, ISSN 1090-0241.

accounts for a substantial recovery in pile bearing capacity and partly compensates for the loss of bonding in sensitive clays (Karlsson et al. 2019). In the final stage of the pile cycle, when the pile is loaded, the pile response depends on the nature of loading and the current state after installation and equalization. Therefore, to accurately describe the spatiotemporal response of deep foundation systems in a finite-element (FE) analysis, the loading history in the clay at all stages before the application of the loads, governed by the state in the soil, need to be considered.

In principle, the installation effects should be incorporated by modeling the complete pile cycle, so that the state in the soil emerges from the analysis (Staubach et al. 2023). More commonly, the new state from the pile installation is obtained from numerical cavity expansion in a small-strain code (Sheil et al. 2015; Abu-Farsakh et al. 2015). The numerical complexity of modeling displacement piles implicitly in FE analysis arises from the following combination of phenomena (Wang et al. 2015; Hunt et al. 2002; Singh et al. 2022):

1. The large deformations around the pile tip during installation call for special considerations;
2. The coupled hydromechanical response of the fine-grained soil with very low hydraulic conductivity close to the pile; and
3. The evolving state of natural clays subjected to large strains, as is the case for pile installation.

So far, not all of the governing processes that emerge in the soil during and after the installation of displacement piles have been modeled in an integrated manner. The rate dependency in fine-grained soils in combination with strain softening was shown to significantly influence the undrained response of cone penetration test (CPTu) penetration (Liyanapathirana 2009). For CPTu and pile installation problems in clay, the installation and equalization stage has been numerically studied using different methods that address or mitigate the issue of large deformations.

Methods used to analyze penetration problems in clay include small deformation approaches, such as numerical cavity expansion (Abu-Farsakh et al. 2015; Rezania et al. 2017; Sheil et al. 2015) and the press and replace method (Sivasithamparam et al. 2015a; Tan et al. 2023) as well as large deformation approaches, such as arbitrary Lagrangian Eulerian (ALE) methods (Sheng et al. 2013; Mahmoodzadeh et al. 2014), coupled Eulerian Lagrangian (CEL) approaches (Hamann et al. 2015; Konkol and Bałachowski 2017; Staubach et al. 2023), the material point method (MPM) (Ceccato et al. 2016), smoothed particle hydrodynamics (SPH) (Bui et al. 2008), and particle finite-element method (PFEM) (Monforte et al. 2021).

In the aforementioned approaches, with the exception of the small-strain methods, including a representative effective stress-based constitutive model with a large number of state variables remains challenging. Only a few contributions combine large deformation analyses with state-dependent constitutive models, with the state variables required to capture the more advanced features of natural soil response (e.g., Monforte et al. 2021). A limited number of studies have included the complete pile cycle when studying the load-displacement behavior of the pile (Abu-Farsakh et al. 2015; Staubach et al. 2023; Tan et al. 2023; Sivasithamparam et al. 2015a); however, none of these studies considered the rate dependency of natural soft soils.

This paper presents a numerical study of the complete pile cycle in a sensitive natural clay. As a major advancement from prior studies, an Eulerian-based hydromechanically coupled code for large deformation analysis is combined with an advanced, effective stress–based rate-dependent constitutive model for natural sensitive clays. This work aims to investigate the feasibility of using an advanced constitutive model for soft soils with a consistent set of model parameters to model the installation and service life of a displacement pile in soft clay. The novelty of the work is that all steps (i.e., laboratory tests, field characterization, pile installation, equalization, and pile load tests) are validated against data from the Bothkennar test site.

Methodology

Numerical Model

The numerical simulation of the pile cycle is performed in a two-dimensional (2D) axisymmetric domain, where the pile is penetrated into the clay at the symmetry axis. For the soil domain, a hydromechanically coupled Eulerian formulation enables the large deformations around the advancing pile tip and the emerging drainage conditions in the clay. The simulations are performed in Tochnog Professional (Roddeman 2024); details on the Eulerian numerical formulation implemented in Tochnog are presented in Crosta et al. (2003). The penetration of the pile is modeled by a series of velocity boundary conditions imposed onto the domain. Practically, a geometric entity, representing an infinitely stiff pile, is gradually expanded downward. Simultaneously, all nodes within the expanded geometry are prescribed with the penetration velocity. Horizontal movement in the nodes is prevented within the pile geometry, and for simplicity, elements with all nodes within the pile geometry are removed from the analysis. This method of modeling the penetration of a pile in an Eulerian formulation is identical to the moving pile method proposed by Dijkstra et al. (2011) in which the details of the method are presented.

Although the numerical simulations do not use any specific regularization techniques, the viscoplastic material response of two of the constitutive models adopted has been shown to have a regularization effect on strain softening materials (de Borst and Duretz 2020). A full bond between the pile and the soil is modeled, with failure in the soil. Thus, a relative displacement between the pile and the clay will occur between the first and second node in the first row of soil elements connected to the pile. In this work, a similar constitutive model as for the rest of the domain is utilized, leading to a rough interface formulation, which is in line with the experimental findings of Lehane and Jardine (1992). If needed, any other constitutive model can be prescribed to capture smooth or rough behavior at the interface. For this modeling approach, the penetration resistance varied from 5% to 10% between smooth and rough interfaces (Isaksson 2022), which agrees with the previous findings (Liyanapathirana 2009).

Constitutive Model

The mechanical response of natural sensitive clays includes destructuration (loss of bonding), evolving anisotropy, and rate dependency (creep) (Leroueil and Vaughan 1990; Burland 1990). Given that the sensitive natural clay near the pile is subjected to different magnitudes of strain rates during the installation, equalization, and loading stages of the pile cycle, a rate-dependent constitutive model is preferred. Furthermore, the model should incorporate the most important features of the behavior of natural clay to track the evolving state in the clay over the pile cycle. The Creep-SCLAY1S constitutive model enables the study of these features in a rate-dependent effective stress–based framework. Creep-SCLAY1S (Sivasithamparam et al. 2015b; Gras et al. 2018) is a rate-dependent elasto-viscoplastic interpretation of the elastoplastic SCLAY1S model (Karstunen et al. 2005), which in turn is based on the Modified Cam-Clay (MCC) model (Roscoe and Burland 1968) but extended to include the effect of anisotropy

Table 1. Features of constitutive models of the SCLAY family

Constitutive model	Anisotropy	Bonding	Creep
MCC	—	—	—
SCLAY1	x	—	—
SCLAY1S	x	x	—
Creep-SCLAY1	x	—	x
Creep-SCLAY1S	x	x	x

and destructuration. As such, the models can be used hierarchically; thus, the effect of anisotropy and destructuration can be individually investigated, as well as the impact of rate dependency, which is controlled by selecting either the rate-independent SCLAY1S model or the rate-dependent Creep-SCLAY1S model. For clarity, Table 1 presents the additional features beyond MCC that are included in the constitutive models used in this study. SCLAY1S and Creep-SCLAY1S are implemented as UMAT libraries that are linked to the Tochnog Professional finite-element code.

A brief introduction of the elasto-viscoplastic Creep-SCLAY1S model is given for the simplified triaxial stress space (p', q'), where $p' = (\sigma'_v + 2\sigma'_r)/3$, $q = (\sigma'_v - \sigma'_r)$, and subscript v refer to the vertical direction and r to the radial direction. For the full description, refer to Sivasithamparam et al. (2015b) and Gras et al. (2018). The total strain $\dot{\varepsilon}$ is decomposed in an elastic $\dot{\varepsilon}^e$ and a viscoplastic (creep) $\dot{\varepsilon}^c$ component, where the dot symbol refers to strain rate, i.e., the differentiation with time. The isotropic nonlinear elasticity of the model is formulated similarly to MCC. The normal compression surface (NCS) separates the large and small rates of creep strain [see Fig. 1(a)] and is defined as a sheared ellipse given by the relation

$$f = (q - \alpha p')^2 - (M(\theta)^2 - \alpha^2)(p'_m - p')p' = 0 \tag{1}$$

where the anisotropy is represented by a scalar α that controls the rotation of the surface with respect to the isotropic stress axis. In a general 3D stress space, the anisotropy is described instead by a tensor. $M(\theta)$ is the lode angle–dependent slope of the critical state line, following Sheng et al. (2000). The size of NCS, specified by the vertical tangent of the surface p'_{mi}, is linked to the size of the intrinsic compression surface (ICS) following Gens and Nova (1993), using the bonding parameter χ as

$$p'_m = (1 + \chi)p'_{mi} \tag{2}$$

The current stress surface (CSS) indicates the magnitude of the current effective stress in the soil by the equivalent mean effective stress p'_{eq}. For comparison, Fig. 1(a) includes the isotropic yield surface of MCC. The model is formulated with three hardening laws, where the volumetric hardening applies to the size of the ICS due to volumetric creep strains (ε_v^c) as

$$dp'_{mi} = \frac{p'_{mi}}{\lambda_i^* - \kappa^*} d\varepsilon_v^c \tag{3}$$

where κ^*, the modified swelling index, and the intrinsic modified compression index λ_i^* are defined in the volumetric strain $\varepsilon_v/\ln(p')$ space [see Fig. 1(b)]. The rotational hardening law is formulated following the SCLAY1 model (Wheeler et al. 2003) as

$$d\alpha = \omega\left[\left(\frac{3\eta}{4} - \alpha\right)\langle d\varepsilon_v^c\rangle + \omega_d\left(\frac{\eta}{3} - \alpha\right)|d\varepsilon_q^c|\right] \tag{4}$$

where $\eta = q/p'$ is the stress ratio, and ω and ω_d control the rate of rotation and the rate of rotation due to deviatoric creep strains, respectively. The hardening law for destructuration follows the SCLAY1S formulation (Koskinen et al. 2002) as

$$d\chi = -a\chi[|d\varepsilon_v^c| + b|d\varepsilon_q^c|] \tag{5}$$

where a and b control the rate of destructuration and the relative rate of destructuration due to deviatoric creep strains, respectively. The model assumes an associated flow rule. The viscoplastic strain rates are calculated as

$$\dot{\varepsilon}_v^c = \dot{\Lambda}\frac{\partial p'_{eq}}{\partial p'} \qquad \dot{\varepsilon}_q^c = \dot{\Lambda}\frac{\partial p'_{eq}}{\partial q} \tag{6}$$

where the rate-dependent viscoplastic multiplier is defined as

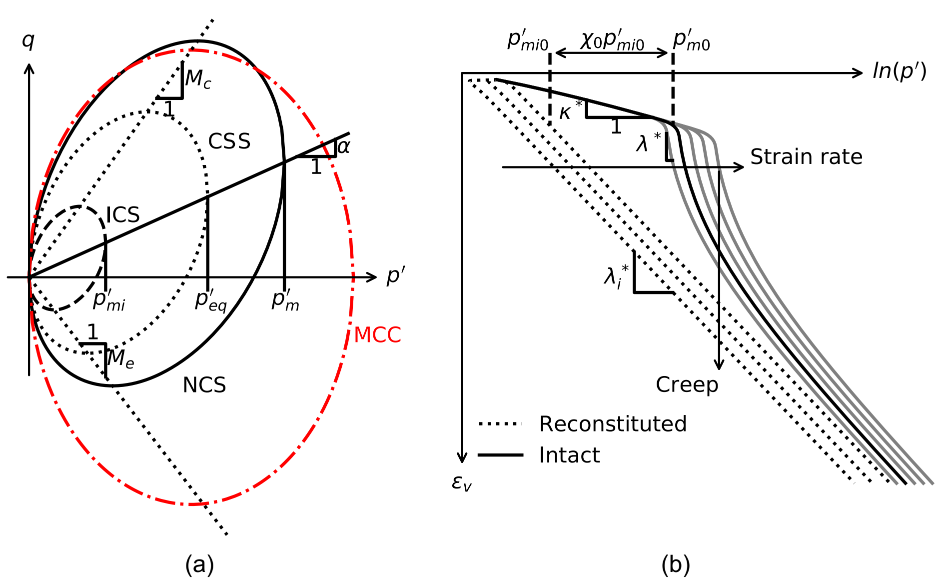

Fig. 1. Illustration of Creep-SCLAY1S model formulation: (a) p'/q; and (b) $\varepsilon_v/(p')$.

J. Geotech. Geoenviron. Eng., 2025, 151(7): 04025061

$$\dot{\Lambda} = \underbrace{\frac{\mu_i^*}{\tau_{\text{ref}}}\left(\frac{p'_{eq}}{p'_m}\right)^{\frac{\lambda_i^*-\kappa^*}{\mu_i^*}}}_{\mathbf{i}} \underbrace{\left(\frac{M^2(\theta)-\alpha^2_{K_0^{nc}}}{M^2(\theta)-\eta_{K_0^{nc}}}\right)}_{\mathbf{ii}} \tag{7}$$

The second term (ii) ensures that the creep strain rate reduces to (i) for odometer loading. The modified creep index μ^* controls the rate-dependent response of the constitutive model. The value for μ^* is most commonly evaluated from odometer tests on a clay sample that is in a remolded state or for a natural clay sample at large stress levels. The reference time τ_{ref} is linked to the strain rate used to obtain the size of NCS. The viscoplastic formulation builds on the concept of isotaches (Šuklje 1957) and is discussed in detail by Grimstad et al. (2010).

The response of the model is illustrated in Fig. 1(b). An increase in strain rate leads to a higher yield stress, whereas deformation under a constant external load, creep, reflects a reduction in strain rate.

Simulation of Bothkennar Site—Investigation Data

The modeled pile tests were conducted at the Bothkennar research site in Scotland; for a detailed overview of the site, see e.g., Nash et al. (1992a) and Hight et al. (2003). Bothkennar clay is a soft, silty clay deposited in estuarine conditions about 6,500–8,500 years ago. The clay has a bulk density ρ of about 1,600 kg m^{-3} in the relevant depths with slightly higher values (1,600 kg m^{-3} to 1,800 kg m^{-3}) in the top 5 m of the deposit. The clay has a water content of around 40% and a liquid limit of around 50% close to the surface, with an increasing trend toward depth up to a value of 60% and 70%, respectively, for clay deeper than ≈4 m. The plastic limit of the clay is about 20%–30%, and the sensitivity is ≈5. The apparent overconsolidation ratio (OCR) is 1.5 for the deeper layers with an increasing value toward the surface that can be modeled with a pre-overburden pressure (POP) of 30 kPa.

The constitutive models were calibrated using the Bothkennar data with the values adopted presented in Table 2. The basic parameters derived based on Nash et al. (1992a) include OCR, POP, coefficient of earth pressure at rest K_0, the vertical k_v and horizontal k_h hydraulic conductivity, and the density of the clay ρ. The slope of the critical state line in compression M_c and in extension M_e are taken from tests on reconstituted soil by Allman and Atkinson (1992). The parameters related to the compression behavior of the clay were based on one-dimensional incrementally loaded compression tests on intact Laval samples (Hight et al. 1992) and reconstituted samples (Nash et al. 1992b). These parameters include the void ratio e_0 and the modified swelling index κ^*, the intrinsic modified compression index λ_i^*, and the modified compression index λ^*. For the models that are formulated without bonding, a choice has to be made on a representative λ^* [see Fig. 1(b)] as these models are unable to capture the evolving stiffness of the soil toward the intrinsic compression index as captured by the models with bonding. The authors chose to evaluate λ^* at stresses just beyond the apparent preconsolidation pressure, thus capturing the initial response just after yielding. The modified intrinsic creep index μ^* was obtained from the secondary compression index in the final load step of the oedometer tests on samples from 9 m depth (Nash et al. 1992b). The duration of the stages used to obtain the OCR from odometer data was approximately 20 h, which gives the reference time $\tau = 0.83$ d. The initial bonding χ_0 was evaluated by comparing the magnitude of effective stress for intact and reconstituted oedometer samples at a stress level slightly below the apparent preconsolidation [see Fig. 1(b)].

The initial anisotropy α_0 of 0.45 was evaluated from investigations on the yielding characteristics of Bothkennar clay by Smith et al. (1992). The calibration of the advanced parameters for the hardening law was conducted on data from triaxial and oedometer tests. The advanced parameters include the parameters a and b for the destructuration law and ω and ω_d for the law that governs the rotation of fabric. The samples for the triaxial tests were trimmed with a wire saw from Laval block samples (Atkinson et al. 1992).

The hierarchical features of the constitutive models link MCC to Creep-SCLAY1S and allow for a consistent set of parameters to be used for all versions of models used. Please note that λ^* should be used instead of the intrinsic value λ_i^* when the analysis does not include bonding. In turn, λ_i and κ should be used instead of λ_i^* and κ^*, for simulations with the SCLAY1S model. The relation between the two parameters is $\lambda^* = \lambda/(1+e)$.

Table 2. Model parameters for Bothkennar clay

Symbol	Parameter	Value
OCR	Overconsolidation ratio	$-/1.5$
POP	Pre-overburden pressure	$30/-$
K_0	Coefficient of earth pressure at rest	0.65
k_h	Hydraulic conductivity (m/s)	1.4×10^{-9}
k_v	Hydraulic conductivity (m/s)	0.7×10^{-9}
ρ	Density (t m^{-3})	1.65
e_0	Initial void ratio	1.85
λ_i^*	Modified intrinsic compression index	0.08
λ^*	Modified compression index	0.177
κ^*	Modified swelling index	0.007
ν'	Poisson's ratio	0.2
M_c	Slope of CSL line in compression	1.4
M_e	Slope of CSL line in extension	1.0
α_0	Initial anisotropy	0.45
ω	Rate of rotation	30
ω_d	Rate of rotation due to deviatoric strains	0.526
χ_0	Initial amount of bonding	5
a	Rate of destructuration	8
b	Rate of destructuration due to deviatoric strain	0.4
μ^*	Modified intrinsic creep index	0.003
τ	Reference time (days)	0.83

Laboratory Tests

Element-level laboratory tests with the calibrated model parameters are compared against the measured triaxial and odometric laboratory tests as part of the calibration process. Strain localization effects and the fully coupled (consolidation) response were not modeled, given the response of the constitutive model is computed at an integration point level.

Fig. 2 shows the simulated response of the undrained triaxial test, using a strain rate of 5%d^{-1}, for a sample from 15 m depth reported by Atkinson et al. (1992). An identical strain rate was used in the test simulations. All the simulations show comparable behavior until yield and agree well with the experimental data. Axial strains ε_a exceeding 30% are required to approach the critical state, as measured for reconstituted samples. The postpeak behavior in the laboratory data shows a considerable strain softening, resulting both from strain localization and (constitutive) material softening, and should therefore not be fully fitted during the calibration process for the response of a single integration point. The two simulations in which the influence of material softening (bonding) is considered capture the measured response best. For these simulations with bonding, an increase in the postpeak excess pore water pressure Δu is computed. Although the pore water pressure increases faster in the laboratory test (as localization is not captured

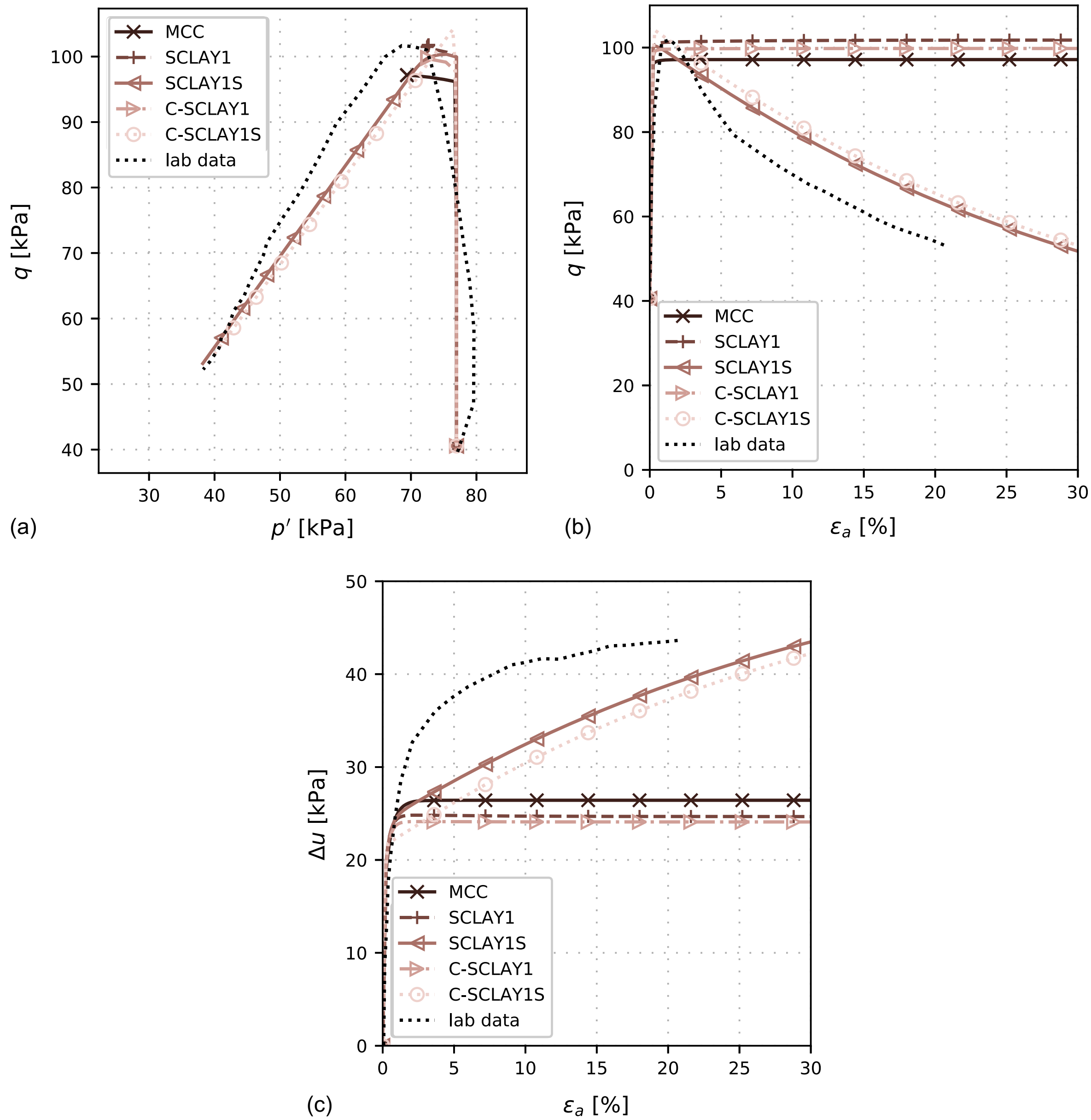

Fig. 2. Triaxial response of Bothkennar clay: (a) mean effective stress p' and deviatoric stress q; (b) axial strain ε_a and deviatoric stress q; and (c) axial strain ε_a and excess pore water pressure Δu. (Data from Atkinson et al. 1992.)

in the numerical analyses), the final magnitude at large strain levels is similar to the results from the numerical simulations. The post-peak behavior is of essence for an accurate description of the installation processes in clay, given the large strains that lead to a remolded state of the soil in the vicinity of the pile.

The results of the numerical simulations of oedometer tests on intact and reconstituted samples are plotted together with the data from laboratory tests on samples extracted from a depth of 5.45 m. The odometer results are normalized with the in situ vertical effective stress σ'_{v0} and presented in Fig. 3(a) for the intact soil and in Fig. 3(b) for the reconstituted soil. Numerically, the reconstituted soil was modeled by setting the χ_0, α_0 to zero and OCR equal to 1. All constitutive models can capture the behavior of the lab tests on intact samples until yielding at the vertical preconsolidation pressure σ'_c. At stresses beyond four times σ'_{v0}, the stress–strain response is not captured by the soil models without destructuration (loss of bonding). This is a direct result of the choice to calibrate the λ^* value for the clay on the initial slope of the compression line after yield rather than fitting the intrinsic value found at large strains in a remolded state. The ability of the models formulated with bonding to capture the evolving stiffness of the intact clay toward the intrinsic response using a single parameter set is an important aspect to capture for the pile installation problem.

The rate-dependent response in the numerical model results in a $\approx$10% increase in yield stress per log cycle of strain for stress paths in odometric and triaxial compression. For comparison, the 1D oedometric yield stress reported by Nash et al. (1992b) changes with approximately 9% per log cycle for samples extracted from 9 m.

CPTu Test

In addition to the simulations of the laboratory tests, a series of numerical cone penetration tests were also performed to investigate the influence of the modeled features on the response of the soft

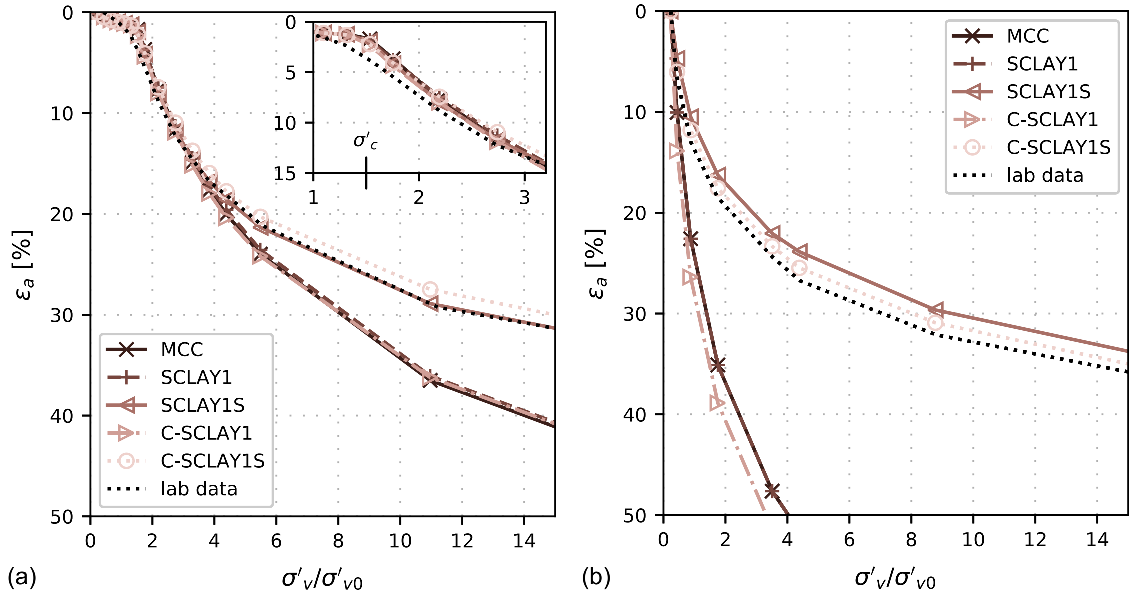

Fig. 3. Odometeric response of Bothkennar clay: (a) intact samples (data from Hight et al. 1992); and (b) reconstituted samples (data from Nash et al. 1992b).

natural clay (see Table 1). The CPTu test was modeled using the numerical framework introduced in the previous section, and the geometry and mesh of the numerical model are presented in Fig. 4 containing 33,359 four-noded quadrilateral elements and 142 three-noded triangular elements in the top left corner of the model (where the cone enters the domain). The mesh density was decided after a convergence study where the reduction in element sides with a factor of 2 resulted in a small change in penetration resistance (< 8%) and excess pore water pressures (< 2%).

A standard 60° cone with a radius R of 18 mm was numerically pushed into the soil with a penetration rate v of 0.02 m s^{-1}. The cone penetration was simulated down to a model depth of 5 m, corresponding to a depth of 6 m in the field test, given that the top 1-m dry crust was included in the model as an overburden load q_0 of 18 kPa. The simulations include the linear increase in the (effective) vertical stress with depth from gravity loading. For numerical stability, the hydraulic conductivity k in the simulation was increased by a factor of 100 for the simulation compared to the values stated in Table 2. Yet, the drainage conditions during the simulation still fall within the undrained regime as indicated by the normalized penetration velocity, i.e., $V = (vD)/c_v \approx 225$ (Mahmoodzadeh and Randolph 2014), where D is the diameter of the penetrometer.

The results from the numerical simulations and the field responses of the CPTu are compared in Fig. 5 using two commonly used soil behavior type (SBT) charts for a depth of 6 m. The tip resistance q_t from the simulations was evaluated by extracting the vertical force on the inclined section of the cone tip divided by the cross-sectional area of the CPTu. The pore pressure was extracted from the soil adjacent to the CPTu corresponding to the position of u_2. The sleeve friction was not considered in the analysis. The field measurements of u_2 and q_t are taken as a mean value from several tests presented by Jacobs and Coutts (1992). The Creep-SCLAY1 and SCLAY1S models deviate most from the field measurement. Creep-SCLAY1 gives the highest penetration resistance and lowest excess pore water pressure, while SCLAY1S gives the lowest pore

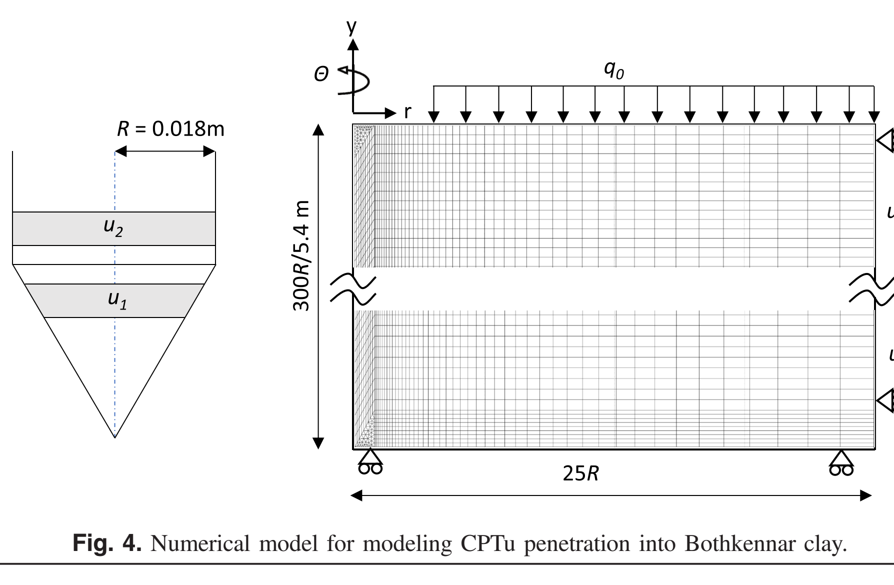

Fig. 4. Numerical model for modeling CPTu penetration into Bothkennar clay.

J. Geotech. Geoenviron. Eng., 2025, 151(7): 04025061

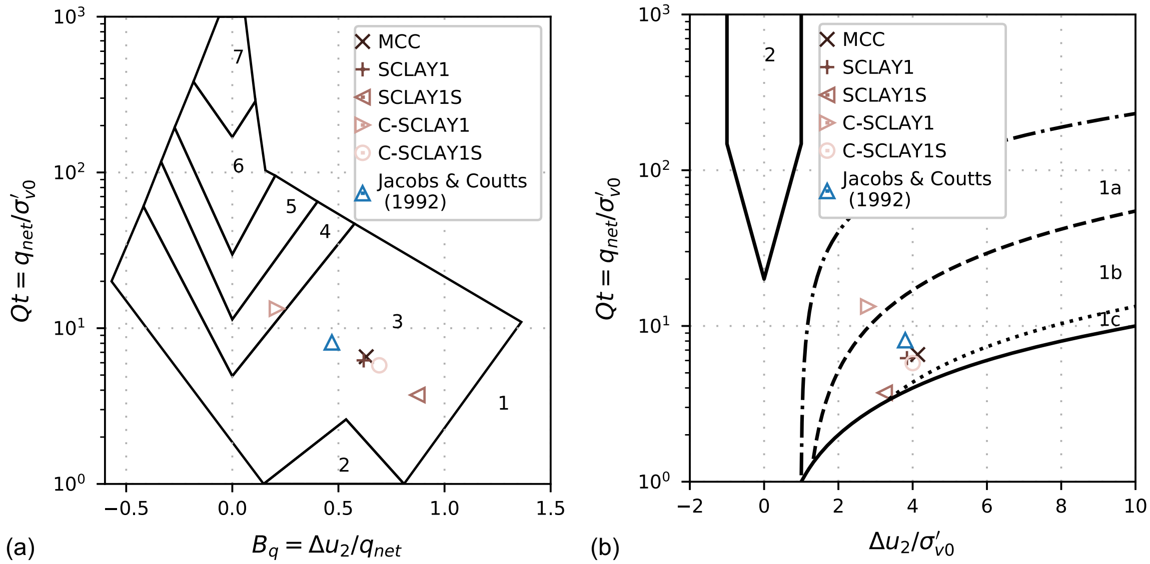

Fig. 5. Simulated CPTu response together with field data from Jacobs and Coutts (1992) plotted on: (a) soil behavior type chart according to Robertson (1990); and (b) soil behavior type chart according to Schneider et al. (2008).

water pressure and penetration resistance. The normalized CPTu response in the SBT gives comparable results for MCC, SCLAY1, and Creep-SCLAY1S, as opposed to the simulated laboratory results where Creep-SCLAY1S and MCC showed large differences in the postpeak behavior.

The CPTu simulations highlight the importance of the interplay between the different (modeled) features of soft natural clays at various strain rates and magnitudes. Including strain softening without including the influence of a rate-dependent soil response (i.e., SCLAY1S) results in a lower resistance than measured in the field. In contrast, including a rate-dependent response without strain softening (i.e., Creep-SCLAY1) gives an overly high resistance. The influence of strain softening and rate dependency seems to compensate each other for the studied soil, as shown by the similarity of results for Creep-SCLAY1S and SCLAY1.

As a final remark, the influence of the anisotropy, as captured by the SCLAY1 model, on the CPTu response for the Bothkennar site is shown to be limited, as indicated by the nearly identical results for SCLAY1 and MCC. The limited influence of the evolution of anisotropy as formulated in SCLAY1 on the penetration resistance is supported by Sivasithamparam et al. (2015a). This limited influence of anisotropy, however, applies to the Bothkennar clay in combination with the anisotropy as captured by the difference between MCC and SCLAY1. In contrast, Moug et al. (2019) finds a more pronounced impact of anisotropy on the numerical penetration resistance in Boston blue clay, OCR = 2.2, where the influence of anisotropy was captured by changing from a model without (MCC) to a model with anisotropy (MIT-S1). The authors believe the main reason for the difference is attributed to the *OCR* combined with the difference in the formulation for the yield surface. The MIT-S1 surface, as formulated by Moug et al. (2019), namely does not allow for stress states at the dry side of critical state, in contrast to Creep-SCLAY1S.

Numerical Modeling of Pile Cycle

The simulations of the CPTu and laboratory tests showed that the Creep-SCLAY1S was the only model able to capture all investigated loading situations satisfactorily. Creep-SCLAY1S was, therefore, the only model used to simulate the pile cycle. The simulation is compared to the data from the installation phase and the subsequent load test of an instrumented pile at the Bothkennar research site (Lehane and Jardine 1994). The data from these tests are used as a benchmark for the numerical analyses.

The pile instrumented by Imperial College (ICP) with a radius of 51 mm and length of 6 m was used (see Fig. 6). The pile was equipped with three instrument clusters, each consisting of two pore water pressure transducers u on opposing sides of the pile, a surface stress transducer, which measured the total radial σ_r and shear stress τ_{ry} at the pile wall, as well as a transducer for the axial load P. The ratio h/R indicates the distance h from the pile tip to the location of the instrument normalized with the pile radius.

The installation was performed from the bottom of a 1-m-deep, cased hole and jacked to a final depth of 6 m or 3.2 m with a

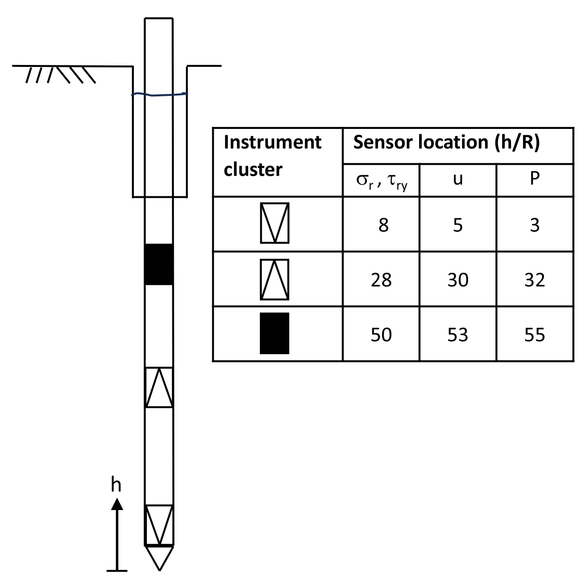

Fig. 6. Schematic illustration of the ICP. (Data from Lehane 1992.)

penetration rate of typically 500 mm/min. Several pause periods were required during the installation, resulting in a total installation time of ≈285 min for one of the 6-m-long piles. After the installation, the pile was left in the soil for equalization of excess pore water pressures before the actual pile load test.

The numerical simulations of the pile installation were conducted using the same numerical method, including the application of velocity boundary conditions directly to the soil, as for the CPTu simulations. Given the resemblance in geometry between the CPTu and the model pile, which also had a cone-shaped tip with an angle of 60°, only minor adjustments were required for the numerical model. The size of the domain was changed, following a sensitivity study on the soil displacement at a radial distance of 5 m from the pile. The final vertical extent of the domain was set to two times the simulated pile penetration depth, and the horizontal extent was set to 3 times the penetration depth. A total of 135,522 four-noded quadrilateral elements and 142 three-noded triangular elements were used. The relation between the radius and the elements close to the pile was kept identical to the mesh used in the CPTu simulation presented in Fig. 4.

The numerical simulation was conducted with a penetration rate of 500 mm/min similar to the field test. No pause periods were included, resulting in a total installation time of 10 min. The simplified modeling of the installation rate without the pause periods is partly compensated by the fact that the hydraulic conductivity in the installation phase had to be increased by 100, similarly to the CPTu simulations, to avoid convergence issues of the coupled simulation. Given that the corresponding normalized penetration velocity was still ≈330, the pile installation is deemed to be performed in undrained conditions. When the pile reached full depth, at the start of the equalization stage, the hydraulic conductivity was set to the value derived from the experimental data reported in Table 2. After reaching the installation depth of 6 m, the pile is kept in a fixed position during the equalization stage for 4.2 days until the start of the loading stage. The displacement-controlled loading was performed in compression with a rate of 10 mm h^{-1}. The modeled conditions during the pile test correspond to the test BK2C reported by Lehane and Jardine (1994).

Installation and Equalization

Fig. 7 presents the radial total stress $\sigma_{r,i}$, pore water pressure u, and the base resistance q_b during pile installation for the numerical simulation and field data from Lehane and Jardine (1994). It appears that for all of the presented measurements, the simulation of pile installation results in lower pressure acting on the pile compared to the field test. However, the gradient of the change with penetration depth is captured well, and the magnitude of the difference between the simulation and field test remains similar for the deeper parts of the pile penetration.

The change of stresses in the soil during the equalization phase is computed as a function of time and presented in Fig. 8 together with the range found in the three instrument positions as presented by Lehane and Jardine (1994). Three different equalization measures are compared:

- degree of consolidation U using excess pore water pressures;
- total stress relaxation $(\sigma_r - u_0)/(\sigma_{r,i} - u_0)$, where σ_r is the current total stress and $\sigma_{r,i}$ is the total stress directly after installation (both corrected by the initial pore water pressure in the soil u_0); and
- the evolution of the radial effective stress; the ratio of the current radial effective stress σ'_r and the radial effective stress at the end of the equalization $\sigma'_{r,c}$.

The consolidation behavior of the soil after installation is modeled correctly, as shown by the predicted U. Similarly, the simulated relaxation of total stress at the pile shaft, ≈50%, agrees well with the values measured in the field. Finally, the development of the relative effective stress on the pile surface is captured reasonably well. The numerical simulation, however, does not reproduce the initial decrease in effective stress found in the field test.

Fig. 9 presents the computed radial stresses in the soil directly after installation ($\sigma'_{r,i}$) and after equalization ($\sigma'_{r,c}$). The excess pore water pressure after installation Δu_i is added for comparison. The measured radial effective stress after the equalization stage ($\sigma'_{rc,field}$) and in situ vertical ($\sigma'_{y,0}$) and horizontal effective stress ($\sigma'_{r,0}$) are plotted for a vertical cross-section close to the pile in Fig. 9(a). The predicted radial effective stress is shown to decrease during installation, followed by a regain in magnitude to values slightly higher than the initial value. Therefore, the stress ratio resulting from the simulations ($K_c = \sigma'_{r,c}/\sigma'_{y,0}$) becomes slightly higher than the assumed initial $K_0 = 0.65$ along most of the pile length. Close to the pile tip, however, the K_c increases to a value slightly higher than 1. A pronounced tip effect is also present in the measured field data but extends further from the tip in relation to the simulations. The radial effective stress in the field after consolidation is about the same as the initial vertical effective stress along the shaft before installation. Close to the tip, the measured K_c in the field increases to between 1.2 and 1.45.

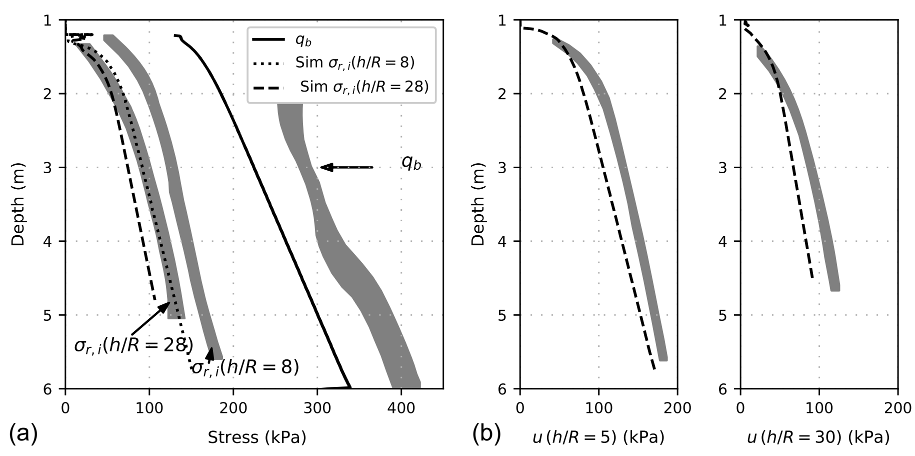

Fig. 7. Stress during pile installation, field data from Lehane and Jardine (1994) indicated by the shaded area: (a) total radial stress; and (b) pore water pressure.

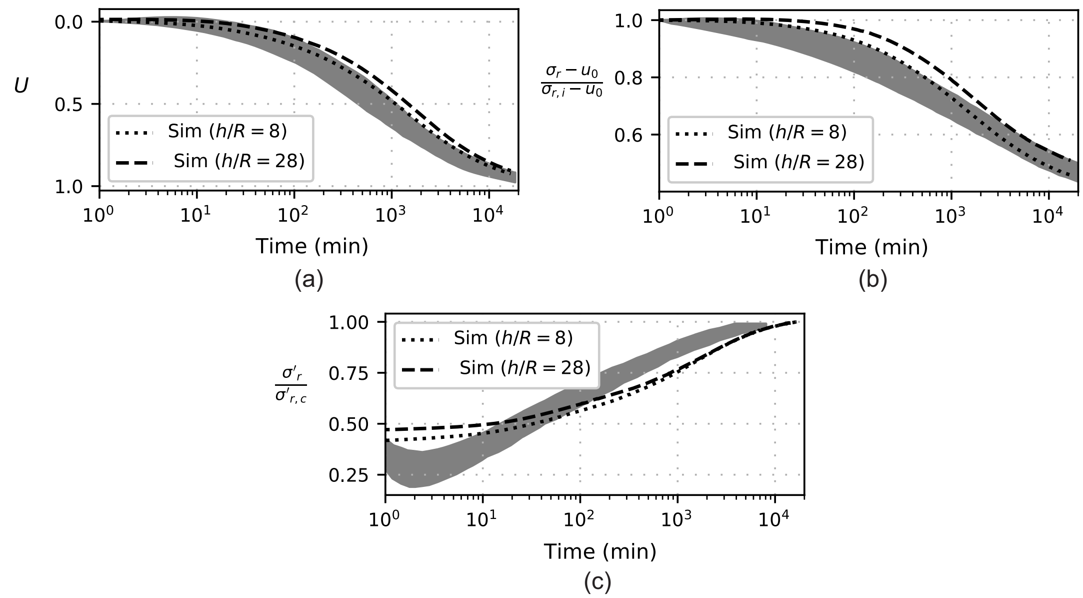

Fig. 8. Equalization of pore water pressures after the end of pile installation. Field data from Lehane and Jardine (1994) indicated by the shaded area: (a) pore water pressure dissipation; (b) total stress relaxation; and (c) development of radial effective stress.

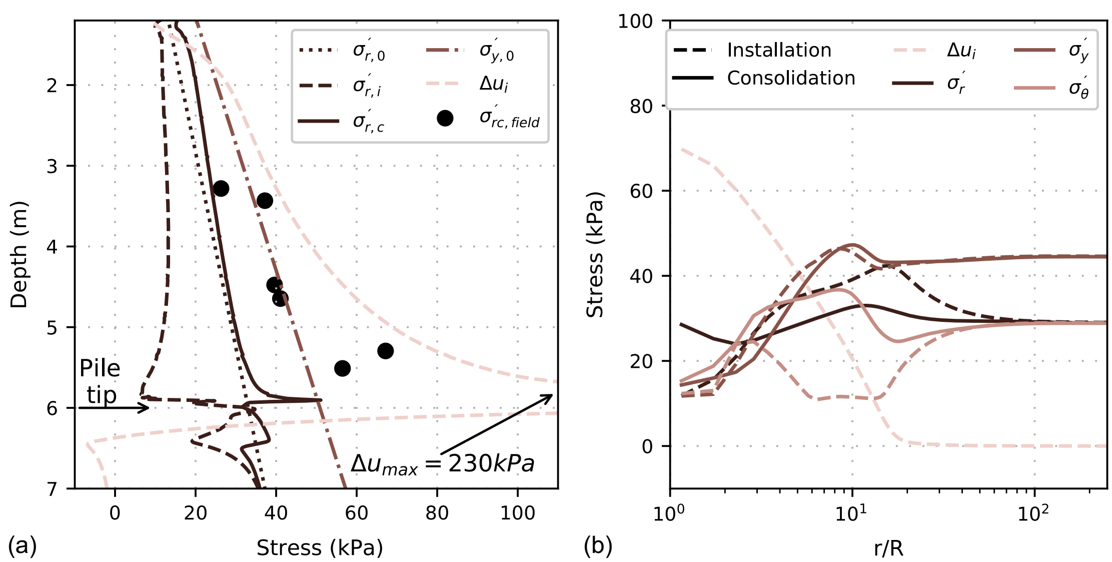

Fig. 9. Stress distribution in soil after installation (dashed lines) and consolidation (solid lines): (a) vertical distribution; and (b) horizontal distribution at 5 m.

The effective stress distribution in the horizontal cross-section at a depth of 5 m is presented in Fig. 9(b). The circumferential effective stresses σ'_θ are included in addition to the stresses in Fig. 9(a). The installation of the pile leads to an increase in pore water pressure up to $\approx 20R$ from the pile, while the effective stress is influenced up to a distance of $\approx 60R$. Directly after installation, all effective stress components are of a similar magnitude close to the pile shaft. However, the dissipation of excess pore water pressures at this location mainly leads to additional effective stresses in the radial direction. At a distance between $3R$ and $10R$ from the pile, the radial effective stress is increasing due to pile installation followed by a reduction in stress to about in situ levels. Interestingly, the vertical effective stress is only marginally influenced by the consolidation.

The influence of the installation and subsequent equalization phase on the fabric anisotropy and degree of bonding in the clay is presented in Fig. 10(a) for the p_m, χ, and α normalized with the initial values. Fig. 10(b) presents the individual values of the components of α. The degradation of bonding χ, controlled by viscoplastic strains, is influenced to a comparable distance to the pore water pressure increase resulting from installation [Fig. 9(b)]. The size of the NCS p_m increased stepwise with the increase of mean effective stress, during the consolidation of the excess pore water pressures and creep in the soil. The consolidation stage does not considerably decrease the degree of bonding in the soil because of the small additional (viscoplastic) strains compared to the large strains that already occurred during the installation stage.

J. Geotech. Geoenviron. Eng., 2025, 151(7): 04025061

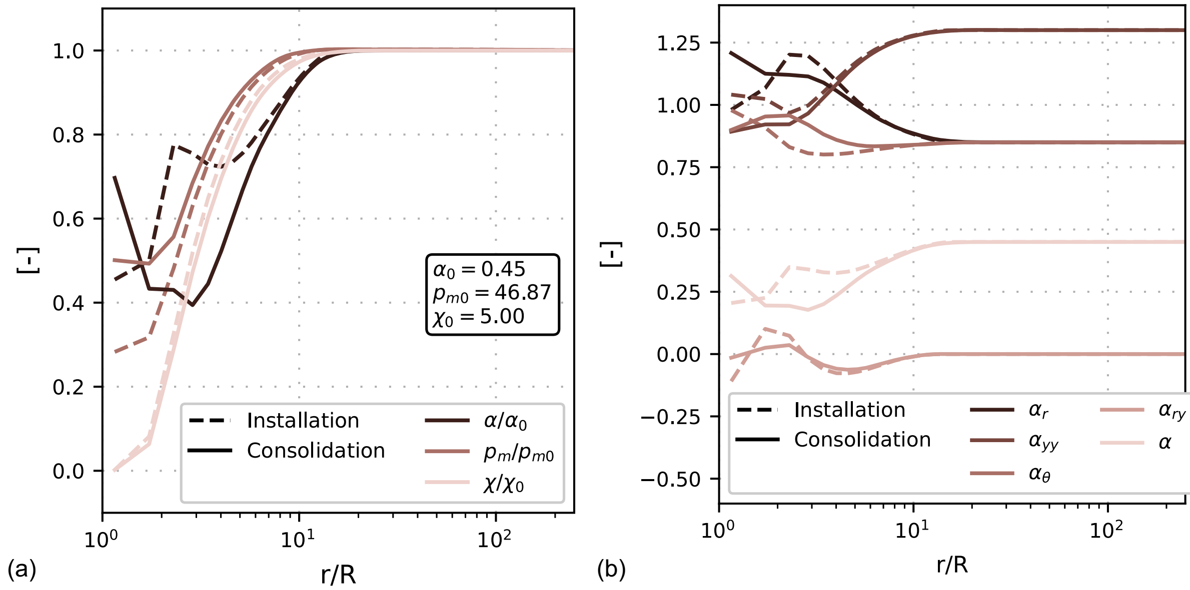

Fig. 10. Horizontal distribution of state variables for Creep-SCLAY1S after installation (dashed lines) and consolidation (solid lines) at a depth of 5 m: (a) state variables; and (b) components of $\boldsymbol{\alpha}$.

The rotation of fabric is first influenced by the installation where the main components of the fabric are close to 1, indicating that NSC becomes almost isotropic. During the consolidation phase, anisotropy develops toward a limit value based on the current stress state in the soil and the deviatoric and volumetric creep strains [see Eq. (4)]. The simulated anisotropy close to the pile after consolidation shows a rotation of the NCS toward σ'_r.

Pile Load Test

The pile load test is simulated following the equalization of excess pore water pressures in the clay. For the numerical simulation, an equalization time of 4.2 days is used, which is comparable to the field test BK2L1 reported by Lehane (1992). The loading rate during the pile load test in the numerical simulation was set to $10\ \mathrm{mm\,h^{-1}}$, while the field test specifies a loading of 1 h to failure. Fig. 11 presents the changes in stresses during pile loading. The postpeak pore water pressures measured in the field are not included as they are considered "anomalously low" and considered unreliable by Lehane and Jardine (1994). The radial effective and total stresses and the shear stress at the pile shaft τ_{ry} are numerically extracted from the soil at the vertical position of each individual instrument position as specified in Fig. 6.

The change in total radial stress $\Delta\sigma_r$ is small, less than 5 kPa in both the numerical simulations and the field test. For the simulations, the largest reduction is found for the $h/R = 8$ and the smallest in the $h/R = 50$ position, while an opposite trend is shown in the field tests. The authors cannot say with certainty what is the origin of this difference as it could be both uncertainties arising

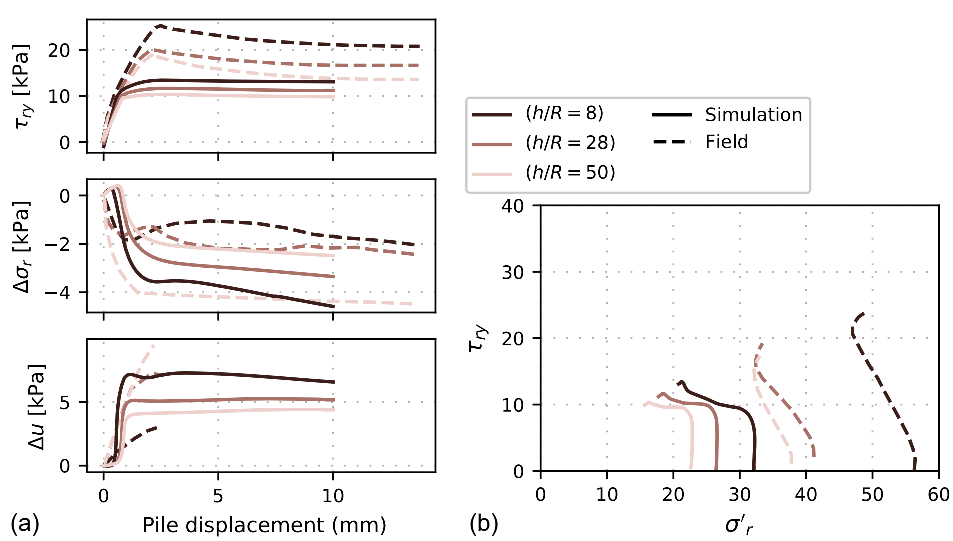

Fig. 11. Stress at shaft during pile loading measured in the field (dashed lines) and from the numerical simulations (solid lines): (a) stress change; and (b) stress path. (Data from Lehane 1992.)

from the measurements and aspects of the problem not captured by the numerical simulation.

Fig. 11(b) presents the effective stress path during pile loading for the numerical simulations and field test. The postpeak field response is excluded following the unreliable pore pressure readings. The small change in radial total stress during pile loading is equal between the simulation and field test, while the shear stress is lower for the numerical simulation, which follows the lower initial radial stress at the start of the pile load test. The numerical simulations show a constant effective stress until pore water pressures build up, indicating yielding. After the point of yielding, the radial effective stress decreases which partly results from a decrease in total pressure (about 2 kPa to 4 kPa) and the increase in pore water pressure (about 4 kPa to 7 kPa).

Sensitivity Study

A sensitivity study was conducted to investigate the impact of consolidation time, loading rate and loading direction on the pile response. Additionally, one simulation was performed where the pile was wished in place (WIP) to investigate the impact of including the installation and equalization stage in the modeling of pile behavior. The various simulations performed as part of the sensitivity study are summarized in Table 3.

The influence of loading direction on the pile load response is presented in Fig. 12(a). The computed stress paths in compression and tension are similar until reaching failure, after which a slight decrease in effective stress is found for the pile loaded in compression and a slight increase in tension. The stresses at failure are similar in magnitude for the two loading directions. The impact of the installation and equalization phase in the numerical analyses of piles is shown in Fig. 12(b). WIP shows a higher peak shear stress upon loading but experiences a very brittle (strain softening) behavior postpeak. This observed brittle behavior results from the gradual remolding of the (intact) clay during shearing, resulting in lower residual stress compared to the results that include the modeling of the installation and equalization stage. For the simulations that include the full pile cycle, the loss of shear stress due to degradation of bonds and fabric rotation in the soil already occurred during installation, shown in Fig. 10.

Fig. 12(c) shows the result when the equalization time after pile installation is set to 4.2 days, 11.6 days, and 116 days, respectively. Interestingly, the radial effective stress increases from 4.2 days to 11.6 days, due to ongoing consolidation, see Fig. 8(a). In contrast, between 11.6 days and 116 days the equalization process is mainly governed by creep and relaxation processes in the system, as indicated by the slight reduction in the effective radial stress combined with an increase in p_m of about 10% to 15% resulting in a larger shear stress of about 9% at failure. Lehane (1992) reports a continuation of gain in shaft capacity after the end of consolidation of about 18% for a pile retested after 32 days even though consolidation was fully developed before the first load test.

The influence of the loading rate is illustrated in Fig. 12(d), where the pile is installed and left 11.6 days for equalization and tested with a total displacement of 10 mm with a velocity of 100 mm h^{-1}, 10 mm h^{-1}, and 1 mm h^{-1}. A higher loading rate gives higher peak shear stress, about 5% when increased from 1 mm h^{-1} to 10 mm h^{-1} and 10% when increased from 10 mm h^{-1} to 100 mm h^{-1}. For comparison, Lehane (1992) reports an increase of about 6% when the loading rate is increased from 1 mm/min to 10 mm/min. The stress paths for different loading rates are similar. However, a lower rate leads to an earlier decrease in radial effective stress compared to a higher rate. This is the result of the combined effect of the generation of excess pore water pressures and the mobilization of shear resistance, which are both rate-dependent. Both the peak and residual stress are shown to be influenced by the loading rate of the pile.

The relation between the shear stress and the radial effective stress at the shaft is constant for different loading rates, equalization times, and installation effects. The relation corresponds to a friction angle of 32.4° compared to the friction angles in critical state compression 32.6° and tension 25.5°. This provides numerical evidence that the change in emerging shaft resistance is attributed to the evolving radial effective stress at the pile shaft during installation, equalization, and loading.

Table 3. Simulations in the sensitivity study

Equalization time (days)	Loading rate (mm h^{-1})	Loading direction	Installation
0.012	10	Compression	Yes
0.12	10	Compression	Yes
1.2	10	Compression	Yes
4.2	10	Compression	Yes
11.6	10	Compression	Yes
116	10	Compression	Yes
11.6	100	Compression	Yes
11.6	1	Compression	Yes
0.12	100	Compression	Yes
0.12	1	Compression	Yes
11.6	10	Tension	Yes
—	10	Compression	No

Modeling Pile Design Methods

The results from the simulations of the full pile cycle presented in the sensitivity study were compared to commonly used design approaches for pile capacity. Fig. 13 shows the mean shaft resistance from the conducted simulations of pile installation for a variation of equalization times and loading rates, which are normalized with the in situ shear strength (α_s method) and the vertical effective stress (β method) in the simulations. The equalization time and setup time are considered equal in this work and start from the end of pile installation. The same in situ shear strength as Lehane and Jardine (1994) was used to calculate α_s, which was based on unconsolidated, undrained tests on 100-mm-diameter piston samples with a strain rate of 6.5% per day. The mean shaft resistance from the simulation data was based on the sum of the forces acting along the pile shaft normalized with the total area of the shaft. The degree of consolidation U, at the $h/R = 53$ position, indicates that the gain in shaft capacity also continues after the dissipation of the excess pore water pressures. The field test by Lehane (1992) reported values about 20% higher than in the numerical simulations, i.e., $\alpha_s \approx 1$ and $\beta \approx 0.5$.

Lehane et al. (2022) propose the following relation between the CPTu cone resistance at a specific depth q_t to the local shaft capacity of a pile τ_f at that depth:

$$\tau_f = 0.07 F_{st} q_t \max[1, (h/D)]^{-0.25} \tag{8}$$

where h is the distance from the tip of the pile to the specific shaft location and D is the diameter of the pile. F_{st} is set to 1 for clays found in SBT Zone 3 [see Fig. 5(a)]. The proposed relation between CPTu and pile response was investigated using the numerical CPTu and pile load test response presented in this paper. Fig. 14 includes the distribution of shaft resistance estimated using Eq. (8) and the q_t extracted from the numerical simulation of the CPTu using the

J. Geotech. Geoenviron. Eng., 2025, 151(7): 04025061

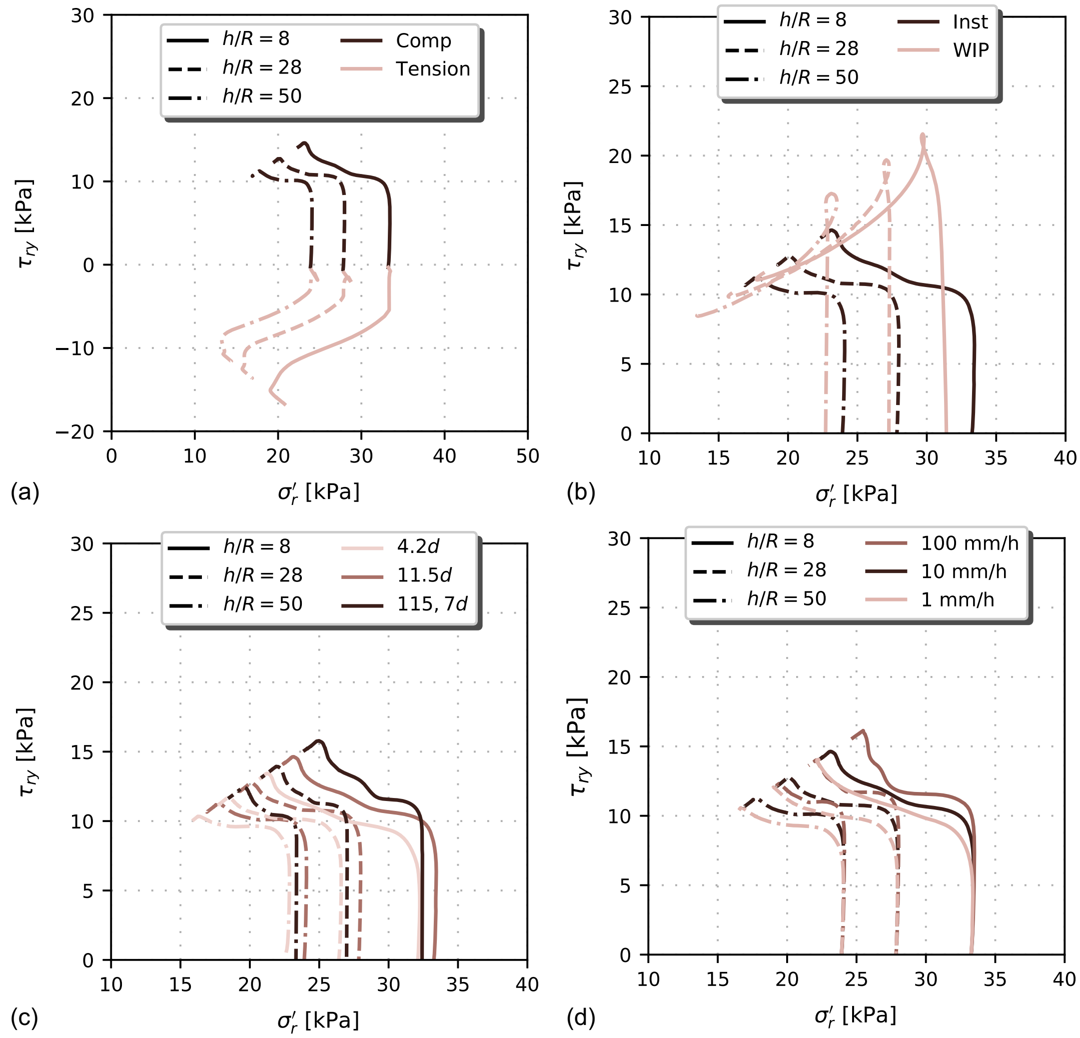

Fig. 12. Sensitivity study stress path: (a) loading direction; (b) installation effect; (c) equalization time; and (d) loading rate.

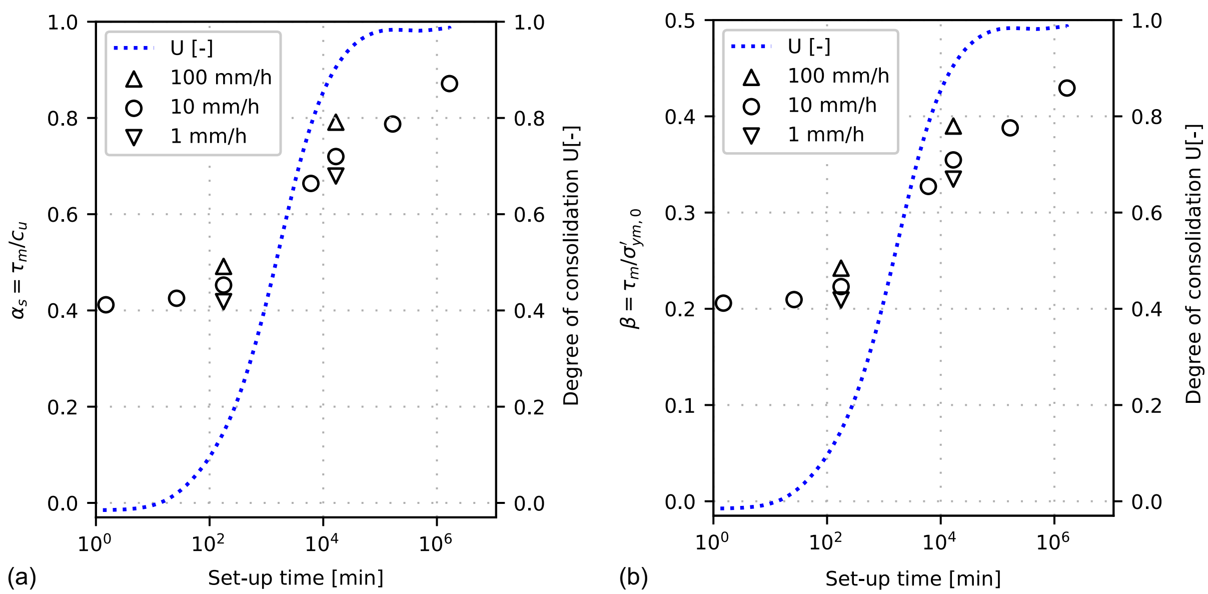

Fig. 13. Influence of loading rate and setup time on the pile shaft capacity: (a) simulated α_s; and (b) simulated β.

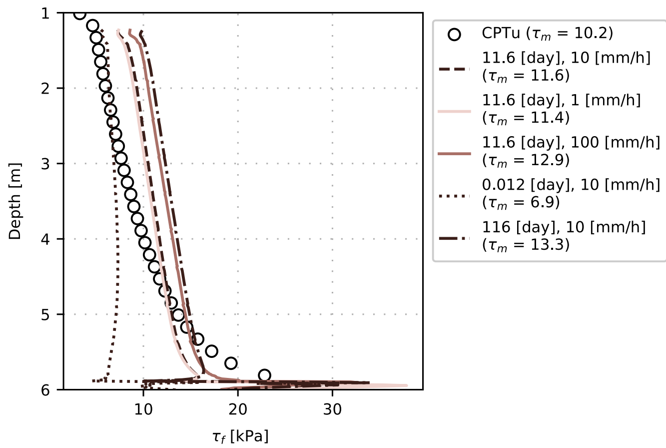

Fig. 14. Shaft capacity predicted from simulation of CPTu test using the correlation proposed by Lehane et al. (2022) and from a numerical pile load test.

Creep-SCLAY1S model and the shear stress from the numerical simulation of the pile load tests. The shear stress from the pile load tests was extracted from the simulations from the first row of soil elements at the pile shaft at the end of the displacement loading (10 mm). Fig. 14 includes the results from five simulations using different equalization times and loading rates, as the degree of consolidation and loading rate influence the emerging response of the numerical pile load test.

The results indicate that the relation proposed by Lehane et al. (2022) is valid for the numerical simulations of the CPTu in this paper but also indicates the relative influence of setup time and loading rate that is not captured by the empirical relation.

Discussion

The results show that the Creep-SCLAY1S model captures the relative influence of destructuration, anisotropy, loading rate, and equalization time for piles installed in sensitive natural clay. As opposed to prior work (Abu-Farsakh et al. 2015; Tan et al. 2023), the strength of this work is that the Class B prediction of the pile load test captures the emerging rate effects with a consistent set of model parameters. In particular, the ability of the model to bridge the low strain rates in laboratory tests and high strain rates of the CPTu is highly promising.

The magnitude of total radial stress acting on the pile, however, is consistently lower in the numerical predictions compared to the field measurements. The lower total stress also results in a lower radial effective stress than measured after equalization, as the relative effect of equalization is captured well by the numerical model (Fig. 8). The prediction of the effective stress is a key aspect in capturing the pile capacity, given the capacity of the pile is governed by the development of radial effective stresses on the shaft.

The remaining differences between the numerical predictions of the pile test and the field measurements, most probably stem from the following factors:

- The first issue is the simplified calibration at integration point level, which is less accurate for the postpeak softening regime where localization effects become more important. Testing, modeling, and calibration in this regime remain challenging both in laboratory and simulations (Singh et al. 2023). Boundary-level simulations of the laboratory tests combined with local stress and strain information from the postpeak regime have great potential to considerably improve the calibration of the model parameters, especially the parameters controlling the destructuration process.
- The pile test in the field and CPTu are performed in the actual natural soil in situ, while the model parameters are derived based on laboratory tests. The quality of the laboratory data from Bothkennar is impacted by the sample quality (which includes sample transport, storage, and trimming) and age (the time between sampling and testing). The samples were not in the highest quality category when assessed with the sample quality metric of Lunne et al. (1997).
- The well-known similitude between CPTu and pile response assumed in design methods, corroborated in our simulations, could be used to optimize the model parameters initially derived based on laboratory tests. Combining numerical forecasting models, such as the one presented herein, with Bayesian updating, e.g., using data assimilation (Amavasai et al. 2024), is a promising intermediate step prior to modeling the pile installation process.

Conclusions

This paper introduces a framework for modeling the full pile cycle of displacement piles in sensitive natural clay. Therefore, a first step is provided toward including the spatiotemporal response of the clay during the pile cycle in system-level geotechnical analysis. The comparison of the numerical results against laboratory tests, CPTu data, and a pile load test from the Bothkennar test site corroborates the validity of the proposed method. The following should be carefully considered for a successful simulation of the pile cycle of a displacement pile:

- The effect of the installation stage on the subsequent pile response is considerable and, therefore, should be included in the numerical modeling of geostructures. This is especially of concern when advanced models that capture creep, destructuration, and anisotropy are used.
- The numerical simulation shows that consolidation and creep lead to an increase in the shaft capacity of the pile over time. Creep continues to increase the shaft capacity after the end of consolidation. This corroborates prior findings (Karlsson et al. 2019).
- The predicted CPTu response is strongly influenced by the soil features modeled. Rate effects (viscoplasticity) and destructuration have the largest impact on the penetration resistance. In the current CPTu simulations, the strain-rate effects from a higher penetration rate (compared to laboratory tests) appear to balance the softening effects from destructuration at large viscoplastic strains.
- This research reiterates the importance of loading rate for the modeling of geostructures in soft clays and the ability of the method to capture the different loading rates encountered in laboratory tests, piezocone tests (CPTu), and pile load tests.
- The laboratory testing, modeling, and calibration in the postpeak softening regime remains challenging and should be the focus for accurate simulations of the installation and load testing of piles in sensitive natural clays.

Despite the outstanding aforementioned challenges, the possibility of modeling the full pile cycle and tracking the evolving state of the soil surrounding a displacement pile in a sensitive natural clay has been demonstrated. Therefore, a viable approach is provided for further studies on the influence of the stages of the pile cycle on the response of complex geotechnical structures during the lifetime of a geotechnical structure.

Data Availability Statement

All data that support the findings of this study are available from the corresponding author upon reasonable request.

Acknowledgments

The first author acknowledges the financial support provided by SBUF (Development fund of the Swedish construction industry, grants 13614 and 14186), BIG (Better Interaction in Geotechnics; grants A2019-19 and B2019-19 from Swedish Transport Administration), and NCC AB. The work is done as part of Digital Twin Cities Centre that is supported by Sweden's Innovation Agency VINNOVA under Grant No. 2019-00041.

References

Abu-Farsakh, M., F. Rosti, and A. Souri. 2015. "Evaluating pile installation and subsequent thixotropic and consolidation effects on setup by numerical simulation for full-scale pile load tests." *Can. Geotech. J.* 52 (11): 1734–1746. https://doi.org/10.1139/cgj-2014-0470.

Allman, M. A., and J. H. Atkinson. 1992. "Mechanical properties of reconstituted Bothkennar soil." *Géotechnique* 42 (2): 289–301. https://doi.org/10.1680/geot.1992.42.2.289.

Amavasai, A., H. Tahershamsi, T. Wood, and J. Dijkstra. 2024. "Data assimilation for Bayesian updating of predicted embankment response using monitoring data." *Comput. Geotech.* 165 (Apr): 105936. https://doi.org/10.1016/j.compgeo.2023.105936.

Atkinson, J. H., M. A. Allman, and R. J. Böese. 1992. "Influence of laboratory sample preparation procedures on the strength and stiffness of intact Bothkennar soil recovered using the Laval sampler." *Géotechnique* 42 (2): 349–354. https://doi.org/10.1680/geot.1992.42.2.349.

Azzouz, A., and M. Morrison. 1988. "Field measurements on model pile in two clay deposits." *J. Geotech. Eng.* 114 (1): 104–121. https://doi.org/10.1061/(ASCE)0733-9410(1988)114:1(104).

Bodas Freitas, T. M., D. Potts, and L. Zdravkovic. 2015. "Numerical study on the response of two footings at Bothkennar research site." *Géotechnique* 65 (3): 155–168. https://doi.org/10.1680/geot.13.P.074.

Bozozuk, M., B. H. Fellenius, and L. Samson. 1978. "Soil disturbance from pile driving in sensitive clay." *Can. Geotech. J.* 15 (3): 346–361. https://doi.org/10.1139/t78-032.

Bui, H. H., R. Fukagawa, K. Sako, and S. Ohno. 2008. "Lagrangian meshfree particles method (SPH) for large deformation and failure flows of geomaterial using elastic-plastic soil constitutive model." *Int. J. Numer. Anal. Methods Geomech.* 32 (12): 1537–1570. https://doi.org/10.1002/nag.688.

Burland, J. 1990. "On the compressibility and shear strength of natural clays." *Géotechnique* 40 (3): 329–378. https://doi.org/10.1680/geot.1990.40.3.329.

Casagrande, A., and S. Wilson. 1951. "Effect of rate of loading on the strength of clays and shales at constant water content." *Géotechnique* 2 (3): 251–263. https://doi.org/10.1680/geot.1951.2.3.251.

Ceccato, F., L. Beuth, P. Vermeer, and P. Simonini. 2016. "Two-phase material point method applied to the study of cone penetration." *Comput. Geotech.* 80 (Jun): 440–452. https://doi.org/10.1016/j.compgeo.2016.03.003.

Crosta, G. B., S. Imposimato, and D. G. Roddeman. 2003. "Numerical modelling of large landslides stability and runout." *Nat. Hazards Earth Syst. Sci.* 3 (6): 523–538. https://doi.org/10.5194/nhess-3-523-2003.

de Borst, R., and T. Duretz. 2020. "On viscoplastic regularisation of strain-softening rocks and soils." *Int. J. Numer. Anal. Methods Geomech.* 44 (6): 890–903. https://doi.org/10.1002/nag.3046.

Dijkstra, J., W. Broere, and O. Heeres. 2011. "Numerical simulation of pile installation." *Comput. Geotech.* 38 (5): 612–622. https://doi.org/10.1016/j.compgeo.2011.04.004.

Franza, A., A. M. Marshall, and R. Jimenez. 2021. "Non-linear soil–pile interaction induced by ground settlements: Pile displacements and internal forces." *Géotechnique* 71 (3): 239–249. https://doi.org/10.1680/jgeot.19.P.078.

Gens, A., and R. Nova. 1993. "Conceptual bases for a constitutive model for bonded soils and weak rocks." In *Proc., Int. Symp. on Hard Soils-Soft Rocks*, 485–494. Rotterdam, Netherlands: A.A. Balkema.

Gras, J.-P., N. Sivasithamparam, M. Karstunen, and J. Dijkstra. 2018. "Permissible range of model parameters for natural fine-grained materials." *Acta Geotech.* 13 (2): 387–398. https://doi.org/10.1007/s11440-017-0553-1.

Grimstad, G., S. Degago, S. Nordal, and M. Karstunen. 2010. "Modeling creep and rate effects in structured anisotropic soft clays." *Acta Geotech.* 5 (1): 69–81. https://doi.org/10.1007/s11440-010-0119-y.

Hamann, T., G. Qui, and J. Grabe. 2015. "Application of a coupled Eulerian–Lagrangian approach on pile installation problems under partially drained conditions." *Comput. Geotech.* 63 (Jun): 279–290. https://doi.org/10.1016/j.compgeo.2014.10.006.

Hight, D. W., A. J. Bond, and J. D. Legge. 1992. "Characterization of the Bothkennaar clay: An overview." *Géotechnique* 42 (2): 303–347. https://doi.org/10.1680/geot.1992.42.2.303.

Hight, D. W., M. A. Paul, B. F. Barras, J. J. M. Powell, D. F. T. Nash, P. R. Smith, R. J. Jardine, and D. H. Edwards. 2003. "The characterisation of the Bothkennar clay." In Vol. 1 of *Characterisation and engineering properties of natural soils*, edited by T. Tan, K. Phoon, D. Hight, and S. Lerouiel, 543–598. Rotterdam, Netherlands: A.A. Balkema.

Hunt, E. H., J. M. Pestana, J. D. Bray, and M. Reimer. 2002. "Effect of pile driving on static and dynamic properties of soft clay." *J. Geotech. Geoenviron. Eng.* 128 (1): 13–24. https://doi.org/10.1061/(ASCE)1090-0241(2002)128:1(13).

Isaksson, J. 2022. "A numerical study on mass displacements from piling in natural clay." Accessed March 18, 2025. https://www.sbuf.se/projektresultat/avhandling?id=c731d33b-4911-4246-4a36-08dc07c7bf87&lId=12a96eef-e1d8-45e8-a867-8f6722cab91e.

Jacobs, P. A., and J. S. Coutts. 1992. "A comparison of electric piezocone tips at the Bothkennar test site." *Géotechnique* 42 (2): 369–375. https://doi.org/10.1680/geot.1992.42.2.369.

Karlsrud, K., and T. Haugen. 1985. "Axial static capacity of steel model piles in overconsolidated clay." In *Proc., 11th Int. Conf. on Soil Mechanics and Foundation Engineering (San Francisco)*, 1401–1406. Rotterdam, The Netherlands: AA Balkema.

Karlsson, M., J. Yannie, and J. Dijkstra. 2019. "Modeling aging of displacement piles in natural soft clay." *J. Geotech. Geoenviron. Eng.* 145 (10): 04019070. https://doi.org/10.1061/(ASCE)GT.1943-5606.0002110.

Karstunen, M., H. Krenn, S. Wheeler, M. Koskinen, and R. Zentar. 2005. "Effect of anisotropy and destructuration on the behavior of Murro test embankment." *Int. J. Geomech.* 5 (2): 87–97. https://doi.org/10.1061/(ASCE)1532-3641(2005)5:2(87).

Konkol, J., and L. Bałachowski. 2017. "Influence of installation effects on pile bearing capacity in cohesive soils—Large deformation analysis via the finite element method." *Stud. Geotech. Mech.* 39 (1): 27–38. https://doi.org/10.1515/sgem-2017-0003.

Korff, M., R. Mair, and A. Van Tol. 2016. "Pile-soil interaction and settlement effects induced by deep excavations." *J. Geotech. Geoenviron. Eng.* 142 (8): 04016034. https://doi.org/10.1061/(ASCE)GT.1943-5606.0001434.

Koskinen, M., M. Karstunen, and S. Wheeler. 2002. "Modelling destructuration and anisotropy of a natural soft clay." In *Proc., 5th European Conf. Numerical Methods in Geotechnical Engineering*, edited by Mestat, 11–20. Paris: Presses de l'Ecole Nationale des Ponts et Chaussées.

Lehane, B. 1992. *Experimental investigations of pile behaviour using instrumented field piles*. London: Univ. of London.

Lehane, B., et al. 2022. "CPT-based axial capacity design method for driven piles in clay." *J. Geotech. Geoenviron. Eng.* 148 (9): 1–18. https://doi.org/10.1061/(ASCE)GT.1943-5606.0002847.

Lehane, B., and R. Jardine. 1992. "Residual strength characteristics of Bothkennar clay." *Géotechnique* 42 (2): 363–367. https://doi.org/10.1680/geot.1992.42.2.363.

Lehane, B., and R. Jardine. 1994. "Displacement-pile behaviour in a soft marine clay." *Can. Geotech. J.* 31 (2): 181–191. https://doi.org/10.1139/t94-024.

Leroueil, S., M. Roy, P. La Rochelle, F. Brucy, and F. Tavenas. 1979. "Behavior of destructured natural clays." *J. Geotech. Eng. Div.* 105 (6): 759–778. https://doi.org/10.1061/AJGEB6.0000823.

Leroueil, S., and P. Vaughan. 1990. "The general and congruent effects of structure in natural soils and weak rocks." *Géotechnique* 40 (3): 467–488. https://doi.org/10.1680/geot.1990.40.3.467.

Liyanapathirana, D. S. 2009. "Arbitrary Lagrangian Eulerian based finite element analysis of cone penetration in soft clay." *Comput. Geotech.* 36 (5): 851–860. https://doi.org/10.1016/j.compgeo.2009.01.006.

Lunne, T., T. Berre, and S. Strandvik. 1997. "Sample disturbance effects in soft low plastic Norwegian clay." In *Recent developments in soil and pavement mechanics*, edited by M. Almeida, 81–102. Rotterdam, Netherlands: A.A. Balkema.

Mahmoodzadeh, H., and M. Randolph. 2014. "Penetrometer testing: Effect of partial consolidation on subsequent dissipation response." *J. Geotech. Geoenviron. Eng.* 140 (6): 04014022. https://doi.org/10.1061/(ASCE)GT.1943-5606.0001114.

Mahmoodzadeh, H., M. Randolph, and D. Wang. 2014. "Numerical simulation of piezocone dissipation test in clays." *Géotechnique* 64 (8): 657–666. https://doi.org/10.1680/geot.14.P.011.

Monforte, L., A. Gens, M. Arroyo, M. Mánica, and J. Carbonell. 2021. "Analysis of cone penetration in brittle liquefiable soils." *Comput. Geotech.* 134 (Apr): 104123. https://doi.org/10.1016/j.compgeo.2021.104123.

Moug, D., R. Boulanger, J. DeJong, and R. Jaeger. 2019. "Axisymmetric simulations of cone penetration in saturated clay." *J. Geotech. Geoenviron. Eng.* 145 (4): 04019008. https://doi.org/10.1061/(ASCE)GT.1943-5606.0002024.

Nash, D. F. T., J. J. M. Powell, and I. M. Lloyd. 1992a. "Initial investigations of the soft clay test site at Bothkennar." *Géotechnique* 42 (2): 163–181. https://doi.org/10.1680/geot.1992.42.2.163.

Nash, D. F. T., G. C. Sills, and L. R. Davison. 1992b. "One-dimensional consolidation testing of soft clay from Bothkennar." *Géotechnique* 42 (2): 241–256. https://doi.org/10.1680/geot.1992.42.2.241.

Pålkommisionen. 2023. "Pålstatistik for sverige 2022." Accessed March 18, 2025. http://www.palkommissionen.org.

Randolph, M., J. Carter, and C. Wroth. 1979. "Driven piles in clay—The effects of installation and subsequent consolidation." *Géotechnique* 29 (4): 361–393. https://doi.org/10.1680/geot.1979.29.4.361.

Randolph, M., and S. Gourvenec. 2011. *Offshore geotechnical engineering*. London: CRC Press.

Rezania, M., M. Nezhad, H. Zanhaneh, J. Castro, and N. Sivasithamparam. 2017. "Modeling pile setup in natural clay deposit considering soil anisotropy, structure, and creep effects: Case study." *Int. J. Geomech.* 17 (3): 04016075. https://doi.org/10.1061/(ASCE)GM.1943-5622.0000774.

Robertson, P. 1990. "Soil classification using the cone penetration test." *Can. Geotech. J.* 27 (1): 151–158. https://doi.org/10.1139/t90-014.

Roddeman, D. 2024. "Tochnog Professional user's manual, May 14." Accessed June 4, 2024. https://www.tochnogprofessional.nl/manuals/user/user.pdf.

Roscoe, K., and J. Burland. 1968. "On the generalized stress-strain behaviour of wet clay." In *Engineering plasticity*, 553–609. Cambridge, UK: Cambridge University Press.

Roy, M., R. Blanchet, F. Tavenas, and P. L. Rochelle. 1981. "Behaviour of a sensitive clay during pile driving." *Can. Geotech. J.* 18 (1): 67–85. https://doi.org/10.1139/t81-007.

Schneider, J., M. Randolph, P. Mayne, and N. Ramsey. 2008. "Analysis of factors influencing soil classification using normalized piezocone tip resistance and pore pressure parameters." *J. Geotech. Geoenviron. Eng.* 134 (11): 1569–1586. https://doi.org/10.1061/(ASCE)1090-0241(2008)134:11(1569).

Sheil, B. B., B. A. McCabe, C. E. Hunt, and J. M. Pestana. 2015. "A practical approach for the consideration of single pile and pile group installation effects in clay: Numerical modelling." *J. Geo-Eng. Sci.* 2 (3–4): 119–142. https://doi.org/10.3233/JGS-140027.

Sheng, D., L. Cui, and Y. Ansari. 2013. "Interpretation of cone factor in undrained soils via full-penetration finite-element analysis." *Int. J. Geomech.* 13 (6): 745–753. https://doi.org/10.1061/(ASCE)GM.1943-5622.0000279.

Sheng, D., S. Sloan, and H. S. Yu. 2000. "Aspects of finite element implementation of critical state models." *Comput. Mech.* 26 (2): 185–196. https://doi.org/10.1007/s004660000166.

Singh, V., S. Stanier, B. Bienen, and M. Randolph. 2022. "A viscoplastic recoverable sensitivity model for fine-grained soils." *Comput. Geotech.* 147 (Feb): 104725. https://doi.org/10.1016/j.compgeo.2022.104725.

Singh, V., S. Stanier, B. Bienen, and M. Randolph. 2023. "Calibration of strain-softening constitutive model parameters from full-field deformation measurements." *Can. Geotech. J.* 60 (6): 817–833. https://doi.org/10.1139/cgj-2021-0342.

Sivasithamparam, N., H. K. Engin, and J. Castro. 2015a. "Numerical modelling of pile jacking in a soft clay." In *Computer methods and recent advances in geomechanics*, edited by F. Oka, A. Murakami, R. Uzuoka, and S. Kimoto, 985–990. London: Taylor & Francis.

Sivasithamparam, N., M. Karstunen, and P. Bonnier. 2015b. "Modelling creep behaviour of anisotropic soft soils." *Comput. Geotech.* 69 (6): 46–57. https://doi.org/10.1016/j.compgeo.2015.04.015.

Smith, P. R., R. J. Jardine, and D. W. Hight. 1992. "The yielding of Bothkennar clay." *Géotechnique* 42 (2): 257–274. https://doi.org/10.1680/geot.1992.42.2.257.

Stanier, S. A., and D. J. White. 2019. "Enhancement of bearing capacity from consolidation: Due to changing strength or failure mechanism?" *Géotechnique* 69 (2): 166–173. https://doi.org/10.1680/jgeot.17.T.030.

Staubach, P., L. Tschirschky, J. Machaček, and T. Wichtmann. 2023. "Monopile installation in clay and subsequent response to millions of lateral load cycles." *Comput. Geotech.* 155 (Jun): 105221. https://doi.org/10.1016/j.compgeo.2022.105221.

Šuklje, L. 1957. "The analysis of the consolidation process by the isotaches method." *Proc., 4th Int. Conf. Soil Mechanics Foundation Engineering London*, 200–206. London: Butterworths Publications

Tan, J., S. Gog, and S. Tan. 2023. "Numerical analysis of a jacked-in pile installation in clay." *Int. J. Geomech.* 23 (6): 04023061. https://doi.org/10.1061/IJGNAI.GMENG-7946.

Tavenas, F., and S. Leroueil. 1977. "Effects of stresses and time on yielding of clays." In *Proc., 9th Int. Conf. on Soil Mechanics and Foundation Engineering (Tokyo)*, 319–326. Tokyo: Japanese Society of Soil Mechanics and Foundation Engineering.

Tornborg, J., M. Karlsson, and M. Karstunen. 2023. "Permanent sheet pile wall in soft sensitive clay." *J. Geotech. Geoenviron. Eng.* 149 (6): 05023003. https://doi.org/10.1061/JGGEFK.GTENG-10955.

Torstensson, B. A. 1973. "The behaviour of cohesion pile group in soft clay." In *Proc., 8th Int. Conf. on Soil Mechanics and Foundation Engineering (Moscow)*, 237–242. Moscow: USSR National Society for Soil Mechanics and Foundation Engineering.

Wang, D., B. Bienen, M. Nazem, Y. Tian, J. Zheng, T. Pucker, and M. F. Randolph. 2015. "Large deformation finite element analyses in geotechnical engineering." *Comput. Geotech.* 65 (Sep): 104–114. https://doi.org/10.1016/j.compgeo.2014.12.005.

Wheeler, S., A. Näätänen, M. Karstunen, and M. Lojander. 2003. "An anisotropic elastoplastic model for soft clays." *Can. Geotech. J.* 40 (2): 403–418. https://doi.org/10.1139/t02-119.